The Astronomical Journal, 149:198 (14pp), 2015 June doi:10.1088/0004-6256/149/6/198

METALLICITY DISTRIBUTION FUNCTIONS OF FOUR LOCAL GROUP DWARF GALAXIES*

Teresa L. Ross[1], Jon Holtzman[1], Abhijit Saha[2], and Barbara J. Anthony-Twarog[3]
[1] Department of Astronomy, New Mexico State University, P.O. Box 30001, MSC 4500, Las Cruces, NM 88003-8001, USA; rosst@nmsu.edu, holtz@nmsu.edu
[2] NOAO, 950 Cherry Avenue, Tucson, AZ 85726-6732, USA
[3] Department of Physics and Astronomy, University of Kansas, Lawrence, KS 66045-7582, USA; bjat@ku.edu
Received 2015 January 26; accepted 2015 April 16; published 2015 May 27

ABSTRACT

We present stellar metallicities in Leo I, Leo II, IC 1613, and Phoenix dwarf galaxies derived from medium (F390M) and broad (F555W, F814W) band photometry using the Wide Field Camera 3 instrument on board the *Hubble Space Telescope*. We measured metallicity distribution functions (MDFs) in two ways, (1) matching stars to isochrones in color–color diagrams and (2) solving for the best linear combination of synthetic populations to match the observed color–color diagram. The synthetic technique reduces the effect of photometric scatter and produces MDFs 30%–50% narrower than the MDFs produced from individually matched stars. We fit the synthetic and individual MDFs to analytical chemical evolution models (CEMs) to quantify the enrichment and the effect of gas flows within the galaxies. Additionally, we measure stellar metallicity gradients in Leo I and II. For IC 1613 and Phoenix our data do not have the radial extent to confirm a metallicity gradient for either galaxy. We find the MDF of Leo I (dwarf spheroidal) to be very peaked with a steep metal-rich cutoff and an extended metal-poor tail, while Leo II (dwarf spheroidal), Phoenix (dwarf transition), and IC 1613 (dwarf irregular) have wider, less peaked MDFs than Leo I. A simple CEM is not the best fit for any of our galaxies; therefore we also fit the "Best Accretion Model" of Lynden-Bell. For Leo II, IC 1613, and Phoenix we find similar accretion parameters for the CEM even though they all have different effective yields, masses, star formation histories, and morphologies. We suggest that the dynamical history of a galaxy is reflected in the MDF, where broad MDFs are seen in galaxies that have chemically evolved in relative isolation and narrowly peaked MDFs are seen in galaxies that have experienced more complicated dynamical interactions concurrent with their chemical evolution.

Key words: galaxies: abundances – galaxies: dwarf – galaxies: evolution – Local Group

1. INTRODUCTION

Dwarf galaxies are important constituents of the universe because they are both the most numerous type of galaxy and test beds for examining galactic evolution on small scales. Additionally, dwarf galaxies show varying and extended periods of star formation (SF) over the age of the universe (Weisz et al. 2011b, 2014). One method of examining these populations is through metallicities, specifically through metallicity distribution functions (MDFs). Metallicity measurements of large numbers of stars over the full range of metallicities are crucial in studying the populations of dwarf galaxies because they allow us to construct robust MDFs, examine any structure indicating subcomponents, and measure gradients across the galaxy. The star formation history (SFH), accretion, outflows via supernova (SN) and stellar winds, and galaxy interactions that cause tidal or ram pressure stripping all play a part in shaping the MDF.

The shape of the MDF offers clues to the galaxy's evolution, which can be characterized by fitting them to analytic chemical evolution models (CEMs). The most basic analytic chemical evolution model is a simple closed box, where gas turns into stars and the stars evolve and return enriched gas to the interstellar medium (ISM), which is again formed into stars. In this model no material enters or leaves the system. However, the simple model is often an inaccurate description of the chemical evolution in dwarf galaxies because the simple model overpredicts the number of metal-poor stars (i.e., the G dwarf problem). Semi-analytic CEMs (Lanfranchi & Matteucci 2010; Hendricks et al. 2014) and hydrodynamic simulations (Marcolini et al. 2006, 2008; Revaz et al. 2009) utilize the galactic SFHs of dwarf galaxies and nucleosynthetic yields from SN I and SN II to predict the gas inflow and outflow necessary to match abundance patterns from multiple elements and the overall MDFs. In lieu of these complex models the simple analytic CEMs offer a concise way to quantify and compare the MDFs of different galaxies, providing insight into the enrichment history of galaxies, especially when only modeling the overall MDF of the dwarf galaxy without information on α abundances.

Recent works have examined the stellar metallicities found in dwarf galaxies using medium- and high-resolution spectra on 8–10 m telescopes (Shetrone et al. 2001, 2003, 2009; Tolstoy et al. 2003; Kirby et al. 2011b, 2013; Koch et al. 2013; Starkenburg et al. 2013; Hendricks et al. 2014; Lemasle et al. 2014). These works examine variations in α elements, abundance patterns in the lowest metallicity stars, abundance patterns in *r* and *s* process elements, and the overall MDFs to better understand the processes that are important in chemical evolution, processes that include the SFHs, the IMF, stellar nucleosynthesis, and the timescales for the formation of galaxies. One of the largest samples of stellar metallicities (>3000 stars) comes from Kirby et al. (2011b, 2013) who present spectroscopic MDFs for 15 dSph and 7 dIrs. They also fit their MDFs to analytical CEMs, extended the stellar mass–stellar metallicity relation, and determined that the MDF shapes vary depending on the morphology such that dSphs tend to have narrower MDFs than dIrs.

* Based on observations made with the NASA/ESA *Hubble Space Telescope*, obtained at the Space Telescope Science Institute, which is operated by the Association of Universities for Research in Astronomy, Inc., under NASA contract NAS 5-26555. These observations are associated with program 12304.

Table 1
Observational Data

Galaxy Name	Observation Dates	Total Exposure Time (s)		
		F390M	F555W	F814W
Leo I	2011 Jun 02, Mar 25	21,024	1760	1500
Leo II	2012 Mar 24, 25	10,080	1760	1500
	2013 Mar 30	10,080	…	…
IC 1613	2011 Dec 16, 20	15,720	1200	1224
Phoenix	2012 Jan 30, 31	16,320	1300	1340

While individual spectra of stars in dwarf galaxies provide abundance and kinematic information, they are still difficult to obtain. Spectra of stars in more distant Local Group (LG) objects are limited to small sample sizes by the long exposure times and large telescopes required to make the observations. While spectral targets are limited to the few brightest stars, photometric metallicities probe deeper and thus sample stars that are typically more representative of the metallicity distribution. Photometric metallicities, though not as accurate as spectra, provide measurements for every star in the field, allowing us to increase samples sizes by an order of a magnitude. This allows us to probe galaxies farther out in the LG, especially when using the resolving power of the *Hubble Space Telescope* (*HST*). We obtained *HST* images in metallicity-sensitive filters (F390M), and two wide band filters (F555W and F814W) for four LG galaxies. By measuring every star in the field we can build up larger samples of stellar metallicities in these dwarf galaxies.

In this work we present photometric metallicities of individual stars in four LG dwarf galaxies: Leo I, Leo II, IC 1613, and Phoenix. We chose galaxies that span different morphologies, masses, SFHs, and distances from the Milky Way (MW). Section 2 describes our two methods of measuring the photometric MDFs, including a new synthetic color–color diagram method, which is similar to the synthetic color–magnitude diagram (CMD) method of deriving SFHs. In Section 3 we compare our metallicities to literature values, including recent work with overlapping spectroscopic targets (Kirby et al. 2011b, 2013). In Section 4 we fit the MDFs with CEMs to quantify the enrichment of the galaxy. In Section 5 we present metallicity gradients from the central regions of each galaxy. In Section 6 we discuss implications of our results on theories of galaxy evolution, and conclude in Section 7.

2. OBSERVATION

The Wide Field Camera 3 (WFC3) observations were obtained between 2011 March and 2013 March as part of *HST* proposal 12304. The dates and exposure times of the observations are given in Table 1. We used the reduced images from the STScI pipeline, which performs bias, flat-field, and image distortion corrections. We additionally used a charge transfer efficiency (CTE) correction module provided by STScI.[4] Magnitudes were measured using the point-spread function fitting photometry package DOLPHOT, which is a modified version of HSTphot (Dolphin 2000). The photometric catalog was culled to reject objects based on goodness of fit and profile sharpness as recommended by the DOLPHOT manual.[5]

We adopt reddening and distance values reported in McConnachie (2012) to calculate the absolute magnitudes. All magnitudes are reported in the Vegamag system. Table 2 lists some basic observable quantities for these dwarf galaxies.

3. METHODS

3.1. Deriving Metallicity

The general technique to measure photometric metallicities relates color to metallicity. The stellar properties that control observed colors are metallicity, effective temperature, and surface gravity. However, effective temperature and surface gravity are dictated by the mass, metallicity, and the current evolutionary stage of a given star. For populations of comparable age the color is directly related to the metallicity. However, an individual giant branch star can be redder either because it has higher metallicity or because it is older, leading to a color degeneracy between age and metallicity. For a mixed aged population, the younger giants are hotter and more massive than older giants of the same metallicity so the color–metallicity relation no longer holds.

Using specifically designed *HST* WFC3 filters that separate the effects of metallicity and temperature on color, we can break the age–metallicity degeneracy. The metallicity sensitivity of the (F390M–F555W) color comes from the F390M medium-band filter which covers the Ca H and K spectral features, one of the strongest metal absorption features in the visible spectrum. The temperature sensitive color, (F555W–F814W), uses two broadband filters that cover mostly the continuum.

The color–color diagram (F390M–F555W, F555W–F814W), has been shown to effectively separate the competing color changes due to metallicity and temperature (Ross et al. 2014), breaking the age–metallicity degeneracy. In the color–color diagram the color change between a 12 and 4 Gyr isochrone of the same metallicity is on the order of a few hundredths of a magnitude (demonstrated in Figure 5 of Ross et al. 2014). Therefore, these two colors can be used to measure individual stellar metallicities of populations of mixed ages and abundances, like dwarf galaxies.

3.2. Measuring Individual Stellar Metallicities

We used only giant branch stars with errors less than 0.05 mag in all filters. These error cuts resulted in samples of 3449, 444, 896, and 578 stars for Leo I, Leo II, IC 1613, and Phoenix, respectively.

Stellar metallicities are assigned in the (F390M–F555W, F555W–F814W) color–color diagram where each giant branch star is matched to the closest Dartmouth isochrone (Dotter et al. 2008) in a grid (spaced by 0.05 dex in [Fe/H] and assuming solar [α/Fe]). The isochrones were empirically corrected to align with globular clusters of known metallicities (M92, NGC 6752, NGC 104, NGC 5927, and NGC 6791 with [Fe/H] = −2.30, −1.45, −0.70, −0.40, and +0.40, respectively). The empirical corrections were derived in Ross et al. (2014) using the same *HST* filters used in this study. This method of deriving photometric stellar metallicities from *HST* photometry

[4] We used the alpha version (2013) for the CTE empirical pixel based corrections for WFC3/UVIS CTE located at http://www.stsci.edu/hst/wfc3/ins_performance/CTE/.

[5] The 2014 DOLPHOT 2.0 WFC3 module manual can be found at http://americano.dolphinsim.com/dolphot/.

Table 2
Dwarf Galaxy Properties

Galaxy	R.A.	Decl.	D (kpc)	M_v	r_h (′), (pc)	$M_\star$ ($10^6 M_\odot$)	$M_{\rm Total}$ ($10^7 M_\odot$)	$\sigma^\star$ (km s^{-1})	$M_{\rm HI}$ ($10^6 M_\odot$)	$\sigma^{\rm HI}$ (km s^{-1})	Type
IC 1613	01 04 47.8 s	+02 07 04	721 ± 5	−14.6	6.81, 1496	100	79.5	⋯	65	25	dIr
Phoenix	01 51 06.3	−44 26 41	406 ± 13	−10.1	3.75, 454	0.77	3.3	⋯	0.12	10	dTrans
Leo I	10 08 28.1 s	+12 18 23	254 ± 17	−11.9	3.40, 251	5.5	2.2	9.2	N/A	N/A	dSph
Leo II	11 13 28.8	+22 09 06	233 ± 15	−9.8	2.60, 176	0.74	0.97	6.6	N/A	N/A	dSph

Note. Data are taken from Tolstoy et al. (2009) and McConnachie (2012). McConnachie (2012) reported the stellar mass, $M_\star$, assuming a stellar mass-to-light ratio of 1. Virial masses are reported from Mateo (1998).

was tested against the listed globular clusters and shown to produce metallicities with errors of 0.15–0.3 dex, with larger errors occurring at lower metallicities. See Ross et al. (2014) for full details on the metallicity derivations from colors.

Although each giant branch star is matched to an isochrone grid of [Fe/H] assuming a solar abundance ratio, many stars are known to have α enhancement, especially low-metallicity ones. The colors we measure are a product of [Fe/H] and the α enhancement; therefore, it is more accurate to think of our measurement as an indicator of the total metallicity, [M/H], that represents the intrinsic combination of [Fe/H] and [α/Fe], even though we are matching each star to an isochrone grid of [Fe/H]. Total metallicity, [M/H], and the iron abundance, [Fe/H], are often used interchangeably because they are usually very similar; only in the cases of large abundance variations (e.g., α enhancements) do the two values differ. In Ross et al. (2014) we quantified the amount of color change expected from α enhancements and provide a means of calculating the [Fe/H] if the α enhancement is known.

3.3. Synthetic Color–Color Diagram Method of Deriving MDFs

In addition to measuring metallicities of individual stars based on color, we have also developed a synthetic color–color diagram technique to derive an MDF from photometry. The technique uses isochrones and an initial mass function (IMF) to make a model color–color diagram of the synthetic populations in order to reproduce the observed color–color diagram.

The technique is similar to the synthetic CMD method used to derive SFHs (see Tolstoy et al. 2009). In the CMD the position and number density of stars depend upon the IMF, age, and metallicity. As pointed out by Dolphin et al. (2002), the CMD of any complex stellar system will be a composite of all the individual stellar populations that comprise the system. Therefore it is possible to model a large number of simple stellar populations (SSPs) in various combinations to reproduce the observed data, including the observational errors. The most likely combination of populations of various ages and metallicities that best match the observations will give the SFH.

In the color–color diagram the position and number density of stars depend upon metallicity and the IMF of a population, and is independent of age, unlike a CMD. The synthetic color–color diagram method of deriving MDFs solves for the weights of a given linear combination of populations that equals the observed color–color diagram; the weights from the linear combination give the metallicity distribution of the population. The advantage is that a given population will occupy a locus where the color and number density of stars found at each location within the color–color diagram is dictated by stellar evolution and the IMF (Tolstoy et al. 2009).

To create the synthetic color–color diagrams, a Kroupa IMF (Kroupa 2001) and colors from the Dartmouth isochrones are used to initially populate a grid of Hess diagrams of SSPs. The isochrone colors were empirically corrected following the calibration described in Ross et al. (2014). The grid spans a metallicity range $-2.5 <$ [Fe/H] $< +0.5$ in steps of 0.05 dex. Each SSP Hess diagram was blurred using the measured photometric errors from each dwarf galaxy. The linear combination of SSPs that reproduces the observed color–color diagram are calculated from the array of synthetic Hess diagrams.

The isochrone color spacing and the bin spacing of the Hess diagrams (0.04 by 0.04 mag) require that the metallicity spacing (and subsequent color change) be larger than the Hess bins. In some regions of the color–color diagram isochrones spaced 0.05 dex of [Fe/H] apart have a color change less than 0.04 mag. If the color change is less than the bin size, only one of the weights for the linear combination of isochrones will be positive; the rest will have negative and nonphysical weights. Additionally, in the synthetic color–color diagram, when the synthetic SSPs are blurred by the photometric errors (up to ∼0.07 mag near the bottom of the giant branch), isochrones closer than 0.15 dex produce nonphysical negative solutions. To account for the issues arising from the isochrone color spacing and the bin spacing in the Hess diagrams, we combine the weights from various metallicity combinations to ensure we sample all metallicities equally. We start with the full range of metallicities ($-2.5 <$ [Fe/H] < 0.5, and spacing of 0.05 dex), calculate the linear combination, eliminate the metallicities that have negative nonphysical solutions, and recalculate the linear weights. This leads to uneven spacing in metallicity due to the smaller color separations at low metallicity and larger color spacing at high metallicity. We repeat the calulation with different metallicity spacings (0.1, 0.15, 0.2, and 0.25 dex) and shifts of 0.05 dex in order to fill in the metallicity spacings. The weights from various metallicity combinations are combined to ensure we equally sample all metallicities.

The MDF weights are checked by creating a synthetic color–color diagram to compare to the observations. We examine the residuals between our observed Hess diagram and a synthetic Hess diagram to ensure that >99% of the residuals deviate by less than 3σ of the overall residual within the Hess diagram. The residual Hess diagram is created using the following

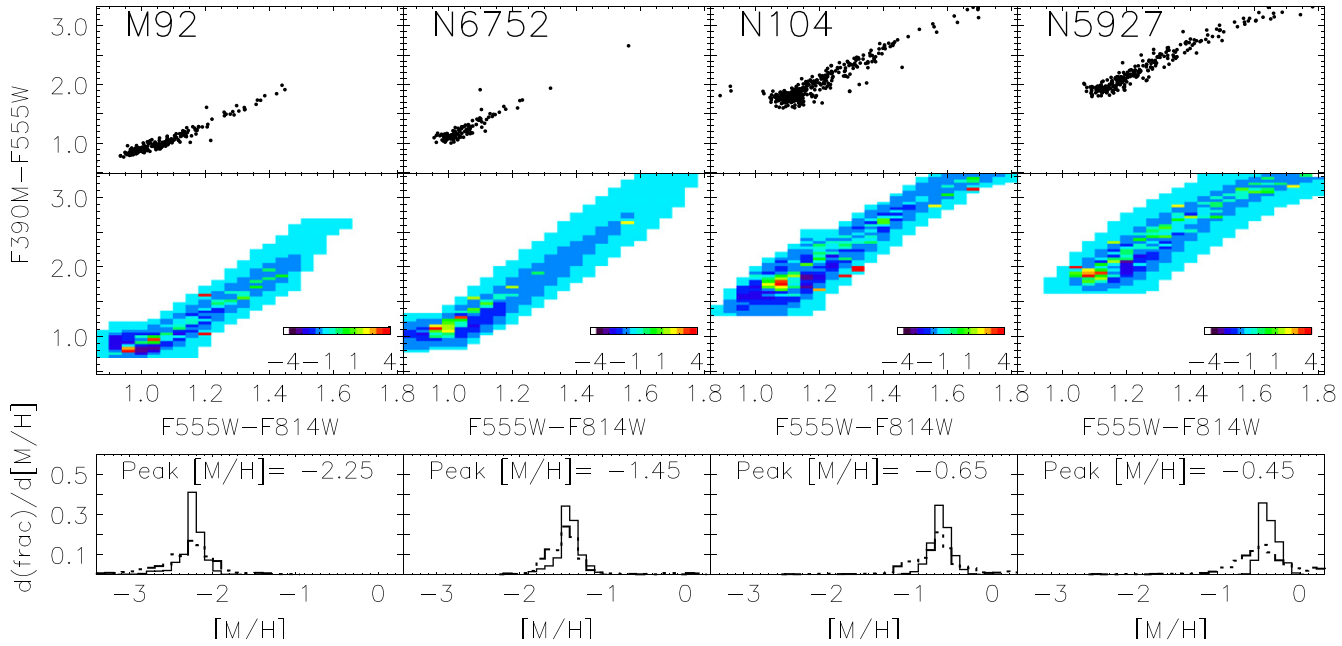

Figure 1. Top panels show the color–color diagrams of giant branch stars in M92, NGC 6791, NGC 104, and NGC 5927. The middle panels show Hess diagrams of the residuals from the observations minus the best combination of synthetic populations normalized to the square root of the synthetic populations. The bottom panels show the MDFs from the synthetic method in solid black as well as the MDF from individually matched stars as dashed lines.

equation:

$$\text{residual Hess diagram} = \frac{\text{observed Hess} - \text{synthetic Hess}}{\sqrt{\text{synthetic Hess}}}. \quad (1)$$

To test the synthetic color–color diagram method of deriving MDFs we performed this analysis on globular clusters of known metallicity, specifically M92, NGC 6791, NGC 104, and NGC 5927, with [Fe/H] = –2.3, –1.45, –0.70, –0.40, respectively. For these GCs we adopted all of the parameters reported in Ross et al. (2014), where the individual MDFs were derived. Hereafter we will refer to the MDFs derived using the synthetic color–color diagram method as "synthetic MDFs," and the MDFs created from individually measured metallicities as "individual MDFs." The synthetic MDFs recovered peak metallicities that are all within 0.05 dex of the literature values. Additionally we find the synthetic distributions to be over two times as narrow as the distributions found from fitting each star individually ($\sigma = 0.15$, 0.19, 0.24, and 0.19 for M92, NGC 6752, NGC 104, and NGC 5927, respectively). The narrower MDFs are expected because this method accounts for the photometric errors, while the individually measured metallicities do not.

Figure 1 shows the process and final results of the synthetic color–color diagram method of deriving MDFs. The top panels display the observed sequence of giant branch stars in the color–color diagram. The middle panels show the Hess diagram of the residuals as described in Equation (1). The bottom panels show the resulting MDFs from the synthetic method (solid line) as well as the individual MDFs (dashed line). The MDFs in the bottom panels illustrate the utility of using the synthetic method over the individual star method, wherein the synthetic MDFs are 30%–50% narrower than the individual MDFs. The synthetic method is statistical in nature, and therefore it does not provide individual metallicities for each star, but rather gives the relative number of stars at each metallicity for the population as a whole.

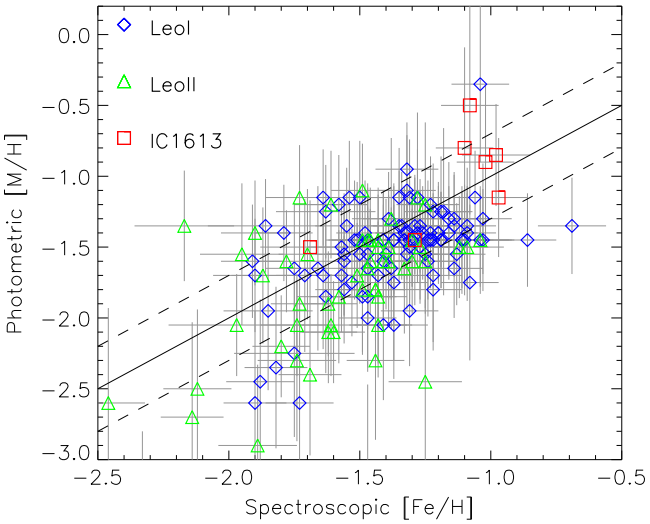

Figure 2. Comparison of photometric and spectroscopic metallicities for 108 stars from Leo I, 54 from Leo II, and 8 from IC 1613, showing that the photometric metallicities deviate to the metal-poor side and the deviations are worse at lower metallicities. Spectroscopic metallicities were measured by Kirby et al. (2011b, 2013).

4. COMPARING METALLICITIES

4.1. Star by Star Metallicity Comparison

In Figure 2 we directly compare the subset of our individually measured stellar sample that overlaps with spectroscopic measurements from Kirby et al. (2011b, 2013). Kirby et al. (2011b, 2013) used medium-resolution spectra and spectral synthesis of Fe I absorption lines to measure metallicities for 814, 256, and 125 stars in Leo I, Leo II, and IC 1613, respectively. Due to the greater spatial extent of their sample we were only able to compare a total of 170 stars: 108 from Leo I, 54 from Leo II, and 8 from IC 1613. The standard deviation of metallicity differences is 0.38 dex, a wider spread

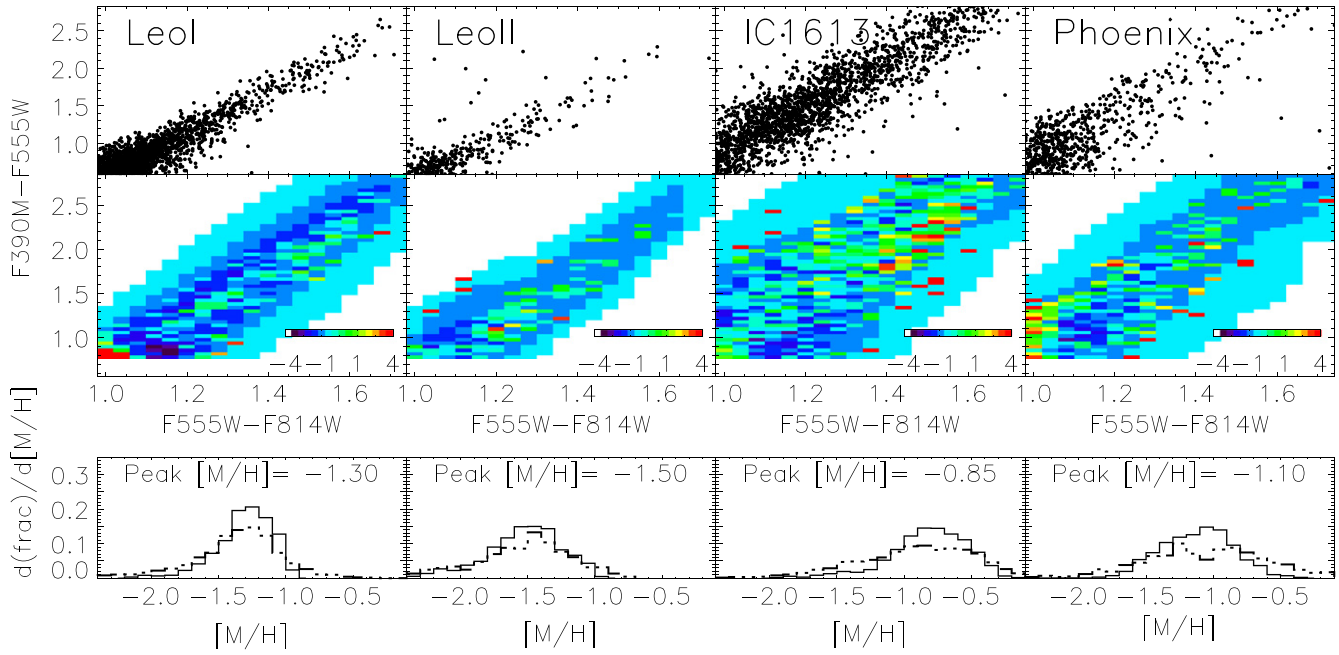

Figure 3. Top panels show the color–color diagrams of giant branch stars in Leo I, Leo II, IC 1613, and Phoenix. The middle panels show Hess diagrams of the residuals from the observations minus the best combination of synthetic populations normalized to the square root of the synthetic populations. The bottom panels show the MDFs from the synthetic method as a solid histogram, while the dashed lines are the MDFs derived from the star individually matched to isochrones.

(by 0.1 to 0.2 dex) than found in the globular clusters from Ross et al. (2014). The larger spread between photometric and spectroscopic metallicity can be partially attributed to the difference in photometric errors between the dwarf galaxies and the globular clusters. The photometric errors along the dwarf galaxy giant branch are two to four times larger than equivalent absolute magnitudes found in the globular clusters, which translates to a δ[Fe/H] of ∼0.1 dex.

The larger spread might also be partially accounted for by α abundance variations. Ross et al. (2014) find that variations in α abundance cause color changes analogous to metallicity changes of a few tenths of a dex (specifically Δ[Fe/H]/$\Delta\alpha$ ∼ 0.65–0.34 across the metallicity range). Without knowing the intrinsic α abundance, and assuming it to be solar, our metallicity measurement will naturally be lower than the actual [Fe/H]. In general, dwarf galaxies tend to show less α enhancement than globular clusters of similar metallicity. Kirby et al. (2011a) find that the α abundance distributions slowly evolve from large α enhancement at low metallicity to roughly solar ratios at [Fe/H] close to a tenth solar. Any α enhancement will cause an underestimate of the metallicity using the photometric method.

In addition to the greater difference between photometric and spectroscopic metallicities, the photometric metallicities deviate more toward lower metallicity. This is not unexpected, as we assign metallicities with an isochrone grid assuming no α enhancements. For any star that has an enhanced α abundance the assigned metallicity from isochrones will be lower than the intrinsic stellar metallicity because the color of a star of solar α abundance will have the same color as an α enhanced star with lower [Fe/H].

The stars with photometric metallicities measured to be [M/H] < −2 tend to be the most discrepant, with differences ⩾1 dex. The main difference is due to the decreasing color change as a function of decreasing metallicity, which means that a small random variation in color for a bluer (metal-poor) star will produce a larger discrepancy in the reported metallicity than the same amount of variation in a redder (metal-rich) star.

4.2. MDF Comparisons

We used the synthetic color–color diagram technique to derive MDFs for the four dwarf galaxies in addition to the individually measured metallicities that were compiled to make MDFs. Figure 3, following the same layout as Figure 1, shows the results from the synthetic MDF derivation method. The top panels show the color–color diagrams for the four dwarfs, the middle panels show the residual Hess diagrams, and the bottom panels show the resulting synthetic (solid line) and individual (dash–dotted line) MDFs. The individual and synthetic MDFs both show similar shapes and peaks, although the synthetic MDFs are narrower, as was noted in Section 3.3 from the MDFs of globular clusters.

For the dwarf galaxies, the average metallicities of the synthetic MDFs are 0.1–0.2 dex more metal-rich than the individual MDFs, although the MDF peaks from the two methods are more closely aligned. Additionally, the globular cluster MDFs from the two methods are not offset. This leads us to believe that the underlying population distribution is causing the offset. For the dwarf galaxies, the difference in average metallicity from the two methods can be attributed to the differences in the metal-poor tails of the MDFs, where the individual MDF has photometric errors that propigate into a wider spread in metallicity. Additionally, the fact that the color change due to metallicity is smaller at low metallicities means that for the same amount of error in color there will be a larger spread in metallicities at low values. The large extent of the metal-poor tail in the individual MDF is the main driver in the offset of the average metallicities for the two methods.

Despite the offset in average metallicity, we believe the synthetic method provides a more accurate MDF shape than the MDF produced by individually measuring metallicities with

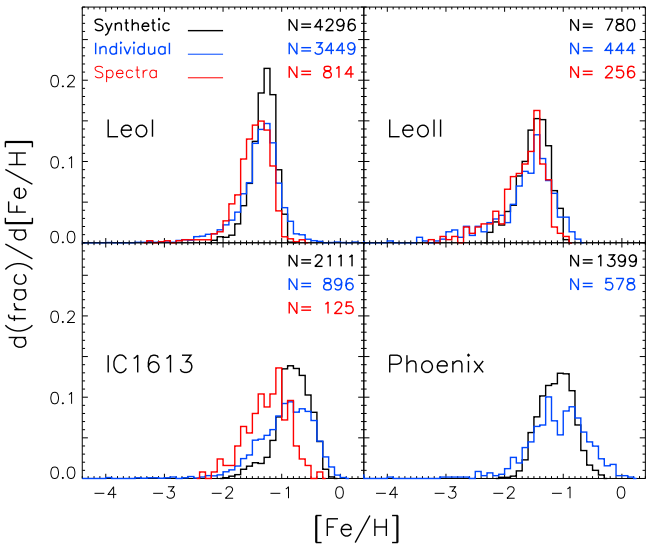

Figure 4. Synthetic MDFs (black lines) compared to the individual MDFs (blue lines). For three of the galaxies, spectroscopic MDFs (red lines) as measured by Kirby et al. (2011b) are also shown as a comparison. The Kirby et al. (2011b) MDFs are true [Fe/H], as opposed to our measurements of [M/H], which are a combination of [Fe/H] and [α/Fe].

isochrone matching. The synthetic method includes stellar sequence information from the color–color diagram, and it systematically accounts for the photometric errors, whereas the individual method relies only on the photometry.

In Figure 4 we compare our two methods of deriving MDFs to the spectroscopic MDFs available from Kirby et al. (2011b, 2013). Table 3 reports the average metallicities, widths, and number of stars measured using the three different MDF derivation methods for each galaxy. The spectroscopic metallicities from Kirby et al. (2011b, 2013) are more spatially extended than our photometric data. Since we are probing a smaller area within each galaxy, it is expected that our MDFs will have some differences compared to the spectroscopic MDFs. The results for each dwarf galaxy are discussed in the following paragraphs.

For Leo I we find $\langle [\mathrm{M/H}]_{\mathrm{individual}} \rangle = -1.43$. The synthetic MDF is narrow ($\sigma = 0.16$), mostly Gaussian with an extension on the metal-poor end, and shows an abrupt cutoff on the metal-rich side of the distribution. The shapes, peaks, and widths are consistent with metallicities found in the literature. Kirby et al. (2011b) found the median, [Fe/H] = −1.42 ($\sigma = 0.33$). Bosler et al. (2007) measured an MDF (for 101 red giant branch (RGB) stars) that peaked at [Ca/H] = −1.34 (σ = 0.21 dex) using the infrared Ca-triplet method of measuring stellar metallicities. Using a different Ca-triplet calibration, Gullieuszik et al. (2009) found [Fe/H] $\simeq -1.37$ ($\sigma = 0.18$ dex) using 54 stars.

For Leo II we find $\langle [\mathrm{M/H}]_{\mathrm{individual}} \rangle = -1.77$ with the MDF showing a more extended tail at low metallicities. The peak value and overall MDF shape are consistent with those reported in the literature. Kirby et al. (2011b) measured an MDF with a peak [Fe/H] = −1.71 from medium-resolution spectra of 256 stars. A near-IR photometric study of RGB stars in Leo II by Gullieuszik et al. (2008) found an MDF peak, [M/H] = −1.64, when they account for the mean age (9 Gyr). Bosler et al. (2007) measured stellar metallicities of 74 stars using the infrared Ca triplet of RGB stars; the MDF they measured peaked at [Ca/H] = −1.65 ($\sigma = 0.17$ dex). Koch et al. (2007a) also measured spectroscopic metallicities using the Ca II infrared method with 52 stars and found the mean metallicity of Leo II to be [Fe/H] = −1.73.

For IC 1613 we find $\langle [\mathrm{M/H}]_{\mathrm{individual}} \rangle = -0.99$, which is more metal-rich than the average spectroscopic metallicity measured by Kirby et al. (2013), $\langle [\mathrm{Fe/H}] \rangle = -1.19$. Another average metallicity measurement from Skillman et al. (2014) finds $\langle [\mathrm{M/H}] \rangle = -1.3$ from an SFH study of a non-central field. The discrepancy between the higher average metallicity that we measure compared to the values reported by Kirby et al. (2013) and Skillman et al. (2014) is partially accounted for by the fact that we are looking at different regions of the galaxy, and thus a younger population of stars. SFHs of IC 1613 show the star-forming regions move continuously inward over the lifetime of the galaxy (Bernard et al. 2007), where SF is associated with higher average metallicity. Additionally, Skillman et al. (2003) find the stellar metallicities of IC 1613 to progress from [Fe/H] = −1.3 to −0.7 over the age of the galaxy. Our field of view looks at the inner ∼5% of the galaxy, while the spectroscopic metallicities are from stars spanning the whole galaxy and the SFH comes from a field 5.′5 from the center. While the average metallicity we find is more metal-rich than most studies, it is more metal-poor than the [Fe/H] = −0.67 found in the high-resolution study based on three supergiants by Tautvaišienė et al. (2007). We believe the average metallicity we measure is reasonable for the young central region of IC 1613 that our field of view covers (∼ 5%) even though it is more metal-poor than the average galactic metallicity measured in other studies.

For Phoenix we find $\langle [\mathrm{M/H}]_{\mathrm{individual}} \rangle = -1.17$.Upon first examination, this average metallicity is in conflict with metallicities reported in the literature, although none of the literature values are spectroscopically derived. Most of the reported metallicities are from SFH studies, like the one by Holtzman et al. (2000) who found $\langle [\mathrm{Fe/H}] \rangle \sim -1.7$. The radial SFH study by Hidalgo et al. (2013) found the old population to have [Fe/H] $\simeq -1.7$, and the younger populations to have [Fe/H] $\simeq -1.2$. Additional studies find [Fe/H] = −1.9, −1.81 ± 0.10 (Ortolani & Gratton 1988; Held et al. 1999). A study of variable RR Lyrae stars in Phoenix predicts $\langle [\mathrm{Fe/H}] \rangle = -1.55$ or −1.75 based on two different period–metallicity relations (Ordoñez et al. 2014). According to the mass–metallicity relationship (Lee et al. 2006), Phoenix, which has the same stellar mass as Leo II, should have a similar metallicity ([Fe/H] ~ -1.7); yet, the average metallicity we measure is higher than the galactic average metallicity reported in other studies.

However, the field of view for our observations covers the innermost region (∼15%) of Phoenix, where SF has occurred as recent as 100 Myr ago and higher metallicities are expected due to the continuous SF occurring in the central region. Additionally, the radial SFH study by Hidalgo et al. (2013) finds the central regions of Phoenix to have a mean metallicity of $\simeq -1.2$, which is in agreement with our results. As with IC 1613, we believe the higher average metallicity we measure reflects the greater amount of enrichment that occurs in the central regions of dwarf galaxies.

5. ANALYTIC MODELS OF CHEMICAL EVOLUTION

The chemical enrichment within galaxies provides information on the gas accretion, gas expulsion, interaction history, and SFH. Matching analytic models of chemical evolution to observations will constrain different evolutionary scenarios. It stands to reason that dwarf galaxies could be represented by

Table 3
MDF Properties

Galaxy	Individual MDF			Synthetic MDF			Spectroscopic MDF		
Name	⟨[M/H]⟩	σ	Num. of stars	⟨[M/H]⟩	σ	Num. of stars	⟨[Fe/H]⟩	σ	Num. of stars
Leo I	−1.43	0.43	3,449	−1.34	0.21	4,296	−1.45	0.32	814
Leo II	−1.77	0.72	444	−1.54	0.27	780	−1.63	0.40	256
IC 1613	−0.99	0.54	896	−0.84	0.30	2,111	−1.19	0.37	125
Phoenix	−1.17	0.67	578	−1.14	0.28	1,399	…	…	…

simple models due to their isolation and relatively less complicated dynamics. Therefore, we begin by fitting a simple model of chemical evolution to our observed MDFs.

The simple model is essentially a leaky box, where gas is allowed to leave the galaxy, but no accretion is occurring. Additionally we assume p is the effective yield, not the true nucleosynthetic yield, where the effective yield is a product of both the amount of metal created, and the amount blown out of the galaxy through winds. The effective yield p is in units of $Z_{\odot}$. The shape of the MDF for the simple model follows the functional form as defined by Pagel (1997):

$$\frac{dN}{d\,[\mathrm{Fe/H}]} \propto \left(10^{[\mathrm{Fe/H}]}\right) \exp\left(-\frac{10^{[\mathrm{Fe/H}]}}{p}\right). \quad (2)$$

The simple model has a tendency to overproduce metal-poor stars, whether in dwarf galaxies or the solar neighborhood. We find that the simple model is often unable to completely reproduce the MDF of dwarf galaxies, in agreement with the findings of Kirby et al. (2011b, 2013). It has been theorized that the paucity of metal-poor stars can be explained by gas infall at later times (Prantzos 2008). Therefore, we also tested an analytical model that includes infalling gas. We fit the "Best Accretion Model" defined by Lynden-Bell (1975), which allows for the gas mass to start small (or at zero), rise to a maximum, then approach zero again as all the mass is accumulated in stars. The accreted gas is assumed to be metal free. Lynden-Bell found a relation between the gas mass, g, stellar mass, s, and total final mass, M, that permits an analytic solution to the differential metallicity distribution (also see Pagel 1997), defined as

$$g(s) = \left(1 - \frac{s}{M}\right)\left(1 + s - \frac{s}{M}\right) \quad (3)$$

where all quantities are in units of the initial gas mass. When $M = 1$ the equation reduces to a closed box where $g = 1 - s$. When M is larger than 1 it essentially becomes a measure of the total amount of gas that has entered the system over the lifetime of the galaxy, so M can be thought of as an accretion parameter. However, it should be noted that while Equation (3) produces the desired MDF shapes, there is no physical rationale behind the actual form of the equation. Equation (3) simply assumes a quadratic relation between gas mass and the stellar mass that peaks then decays as a function of stellar mass. The MDF of the accretion model, as defined by Pagel (1997), follows the form

$$\frac{dN}{d\,[\mathrm{Fe/H}]} \propto \frac{10^{[\mathrm{Fe/H}]}}{p} \frac{1 + s\left(1 - \frac{1}{M}\right)}{\left(1 - \frac{s}{M}\right)^{-1} - 2\left(1 - \frac{1}{M}\right)\frac{10^{[\mathrm{Fe/H}]}}{p}} \quad (4)$$

where s must be solved for numerically from the equation

$$[\mathrm{Fe/H}](s) = \log\left\{p\left(\frac{M}{1 + s - \frac{s}{M}}\right)^2\left[\ln\frac{1}{1 - \frac{s}{M}} - \frac{s}{M}\left(1 - \frac{1}{M}\right)\right]\right\}. \quad (5)$$

For both the simple and the accretion model, the metallicity peak of the model directly increases with p as long as instantaneous mixing of the ISM is assumed. The analytic form of the differential metallicity distribution for these models requires the instantaneous recycling and mixing approximations, where all SN yields are immediately and uniformly returned to the ISM, respectively. The instantaneous recycling approximation does not reproduce the characteristic patterns seen in α element abundances. However α abundances cannot be determined with photometric data alone, and therefore we could not constrain more sophisticated models that account for time-dependent recycling. The analytic models used in this work neglect some of the physics known to be important for galactic chemical evolution; however, these models provide insight into the difference in evolution between galaxies.

5.1. MDF Truncation of the Metal-rich End

For dSphs, one leading hypothesis is that their chemical evolution was interrupted by the removal of gas. This follows from the morphology–density relationship where most dwarf galaxies close to a large primary are dSphs and devoid of gas (Grcevich & Putman 2009; Spekkens et al. 2014). Environmental mechanisms such as tidal stirring and ram pressure stripping have been invoked to transform close satellites from star-forming gas-rich dIrs into quiescent gas-poor dSphs that are found close to a much larger primary (Lin & Faber 1983; Mayer et al. 2001; Grebel et al. 2003; Kazantzidis et al. 2011). Mayer et al. (2006) used simulations to shows that gas-rich dwarfs can be stripped of their gas over a few pericentric passages as they travel through the hot halo of a larger primary. Ram pressure stripping effectively cuts off all SF, stopping the chemical evolution prematurely, likely producing a steep truncation on the metal-rich end of the MDF.

Kirby et al. (2013) show that a sharp metal-rich cutoff of the MDF is primarily seen in dSph type galaxies, not dIrs. Additionally, they added a ram pressure stripping term to the simple chemical evolution model to fit the metal-rich cutoff; however, this model was found to not match well with the dSphs in their sample. Since the accretion models fit all the dSph galaxies better than the simple models, we would like to incorporate a metallicity cutoff into the accretion models that would simulate ram pressure stripping.

Table 4
Chemical Evolution Model Parameters

Galaxy Name	MDF Type	Simple Model	Accretion Model		Accretion + Truncation			Best Model
		p	p	M	p	M	[Fe/H] cutoff	
Leo I	Indiv	$0.054^{+0.008}_{-0.002}$	$0.054^{+0.016}_{-0.026}$	$8.2^{+1.9}_{-2.4}$	$0.050^{+0.020}_{-0.026}$	$7.7^{+1.9}_{-2.2}$	−0.10	A+T
Leo II	Indiv	$0.038^{+0.008}_{-0.006}$	$0.038^{+0.010}_{-0.008}$	$3.0^{+1.3}_{-1.9}$	$0.038^{+0.040}_{-0.008}$	$3.0^{+1.3}_{-2.0}$	−0.40	S
IC 1613	Indiv	$0.228^{+0.041}_{-0.045}$	$0.184^{+0.034}_{-0.032}$	$1.5^{+1.2}_{-0.5}$	$0.182^{+0.036}_{-0.032}$	$1.7^{+1.5}_{-0.7}$	−0.30	A+T
Phoenix	Indiv	$0.118^{+0.015}_{-0.012}$	$0.112^{+0.020}_{-0.014}$	$1.5^{+0.7}_{-0.5}$	$0.112^{+0.027}_{-0.018}$	$1.5^{+1.1}_{-0.5}$	−0.20	A
Leo I	Synth	$0.054^{+0.013}_{-0.010}$	$0.068^{+0.012}_{-0.012}$	$9.8^{+2.1}_{-2.0}$	$0.070^{+0.005}_{-0.005}$	$6.6^{+2.2}_{-2.8}$	−1.0	A+T
Leo II	Synth	$0.036^{+0.044}_{-0.018}$	$0.038^{+0.022}_{-0.016}$	$4.1^{+2.4}_{-2.1}$	$0.038^{+0.050}_{-0.008}$	$4.0^{+2.0}_{-2.4}$	−1.0	A+T
IC 1613	Synth	$0.182^{+0.026}_{-0.082}$	$0.196^{+0.012}_{-0.070}$	$4.1^{+2.0}_{-2.1}$	$0.200^{+0.010}_{-0.036}$	$3.7^{+2.0}_{-1.9}$	−0.40	A+T
Phoenix	Synth	$0.086^{+0.050}_{-0.042}$	$0.092^{+0.058}_{-0.038}$	$3.4^{+2.0}_{-2.4}$	$0.094^{+0.042}_{-0.018}$	$3.3^{+2.6}_{-1.6}$	−0.60	A+T

A more basic approach to testing a metal-rich cutoff is achieved by changing the upper metallicity bounds to a more metal-poor value when integrating the equations of chemical evolution. We ran the simple and accretion CEM with an imposed metal-rich cutoff, truncating the CEM at a lower metallicity than the model would naturally evolve to in order to approximate the effects of ram pressure stripping. A sharp cutoff such as this is somewhat nonphysical, since ram pressure stripping does not immediately remove all gas, and additionally the SF would not be immediately cut off at a particular metallicity across the galaxy. However, this simplistic approach allows us to quickly and efficiently test our models for signs of truncation.

Besides the dSph galaxies, dIrs are expected to have a steeper MDF on the metal-rich side than the CEM predicts. The MDF of a star-forming galaxy should not look like a completed chemical evolution model; rather, the MDF should show a more abrupt cutoff on the metal-rich side because dIrs are still forming stars and enriching their ISM and by definition are not at the end of their chemical evolution. Fitting the CEM with an imposed metal-rich cutoff will also simulate an incomplete chemical evolution, in addition to a CEM that has been halted due to ram pressure stripping.

5.2. Best-fit Models

To find the best model parameters we perform 10^3 trials of the simple model while varying the effective yield, p. We calculate the least squares value between each model and MDF to determine the best parameters for the individual and synthetic MDFs for each galaxy. We also calculate the two-sided confidence interval to find the 1σ range of model parameters. For the accretion model we perform 10^4 trials while varying the effective yield, p, and the extra gas parameter, M. For the accretion + truncation models we run 10^5 trials varying the effective yield, p, the extra gas parameter, M, and the cutoff metallicity. The best-fit parameters for each model and MDF are listed in Table 4.

To fit the individual MDFs the three CEMs have been convolved with a Gaussian with a dispersion equal to the dispersion of the difference between the photometric and spectroscopic metallicities ($\sigma = 0.38$ dex) to account for the spreading of the MDF from the photometric errors. The synthetic MDF method models the photometric errors; therefore we do not convolve the CEM with any additional errors when fitting to the synthetic MDFs.

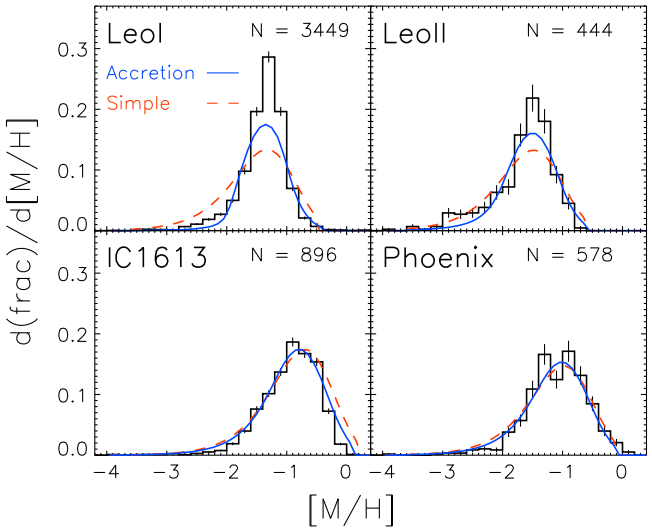

Figure 5. Individual MDFs and Poisson uncertainties shown with the best-fit simple and accretion chemical evolution models. The number or stars in each MDF is listed for each galaxy.

The individual MDFs do not show an abrupt metal-rich cutoff, mostly due to the scatter in metallicity that comes from the photometric technique, as can be seen in Figure 5. However, in the narrower synthetic MDFs we do see truncation of the MDFs on the metal-rich side, indicative of ram pressure stripping. In the accretion model, the larger the M parameter the more the CEM takes on a Gaussian shape. While this is good for fitting the narrow peak of the synthetic MDFs, it does not account for the asymmetry of the extended metal-poor tail and the sharper truncation of the MDF on the metal-rich side as shown in Figure 6. The accretion + truncation model allows for a narrower MDF peak and keeps the asymmetry by truncating the metal-rich side of the distributions, which produces a better model fit for the synthetic MDFs in all four dwarf galaxies, as shown in Figure 7.

5.2.1. Leo I

Leo I is one of the more distant MW companion dwarf spheroidal galaxies (254 kpc, McConnachie 2012); additionally it is receding quickly from the MW ($V_{\rm rad} = 167.9$ km s^{-1}, $V_{\rm tan} = 101$ km s^{-1}, Sohn et al. 2013), making it one of the more unusual dSph galaxies. Since its discovery in the 1950s (Harrington & Wilson 1950) Leo I has been studied by many groups to better understand the SFH, dynamic properties,

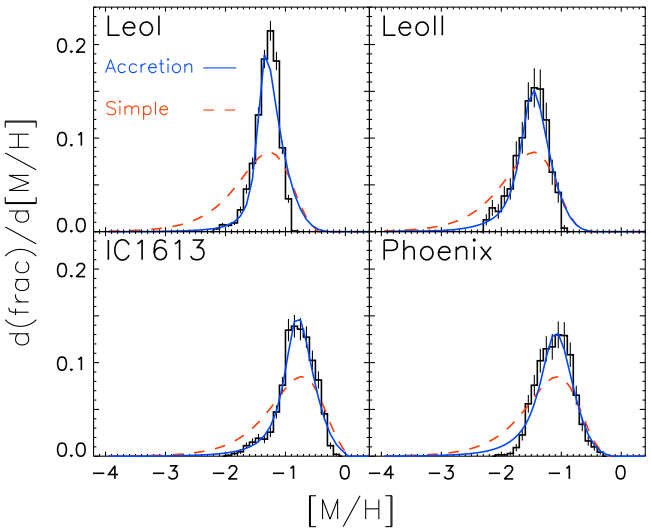

Figure 6. Synthetic MDFs with Poisson uncertainties and the best-fit simple and accretion chemical evolution models are shown. The Poisson uncertainties are calulated from the total number of observed stars modeled by the synthetic color–color diagrams.

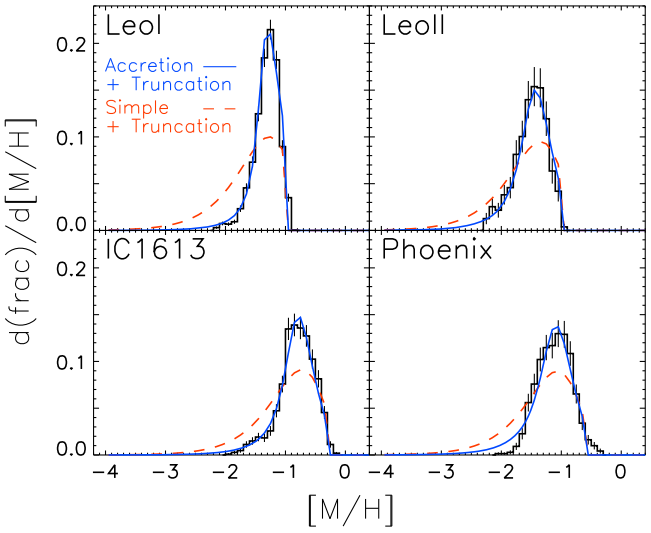

Figure 7. Synthetic MDFs with the Poisson uncertainties shown with the best-fit simple + truncation and accretion + truncation chemical evolution models. The Poisson uncertainties are calulated from the total number of observed stars modeled by the synthetic color–color diagrams.

metallicities, and chemical enrichment history. Here we compare our CEM to results from previous studies.

We find that the accretion + truncation model is the best-fit model for the synthetic MDF. The synthetic MDF shows a narrow peak at [M/H] $\simeq -1.35$, a slight metal-poor tail, and an abrupt cutoff on the metal-rich side of the distribution. The simple model underpredicts the number of stars in the peak and overpredicts the number of metal-poor stars. The accretion model fits the MDF better than the simple model; however this model does not fit the truncation on the metal-rich side of the MDF and subsequently overpredicts the number of metal-rich stars. We find that the narrowness of the synthetic MDF and the metal-rich truncation are best fit by the accretion + truncation models, with a large accretion parameter of $M = 6.60^{+2.2}_{-2.8}$, a yield of $p = 0.07^{+0.005}_{-0.005}$, and a cutoff metallicity of [Fe/H] $= -1.0$.

Kirby et al. (2011b, 2013) also modeled the MDF of Leo I, with a simple, pre-enriched accretion model. They found the accretion model was the best fit, with $M = 7.9$ and $p = 0.043$, which is within the errors but smaller than our accretion model parameter of $M = 9.8^{+3.1}_{-3.0}$, and the yield we derive, $p = 0.068$, is higher than the one they derive, but our MDF has a higher average metallicity (see the discussion in Section 4.2).

Lanfranchi & Matteucci (2010) created detailed CEMs for Leo I and II that use nucleosynthesis for SN I and SN II; an exponentially decreasing accretion parameter; the SFH, α abundances, and the MDF as inputs to solve for the outflowing wind; and the SF efficiency. The detailed chemical evolution model that best matches the Leo I abundances predicts that the galaxy started with a low SF efficiency ($0.6\,\mathrm{Gyr}^{-1}$) for the first 5 Gyr, then had another 7 Gyr episode of SF starting at 9 Gyr with substantial galactic winds throughout (Lanfranchi & Matteucci 2010). The evolution model of Lanfranchi & Matteucci (2010) agrees with the CMD-based SFHs showing that Leo I had slow ancient SF, with an increase in the SFR around 7–8 Gyr ago, and another increase to its highest rate 2–3 Gyr ago, after which the galaxy stopped forming stars 1 Gyr ago (Caputo et al. 1999; Gallart et al. 1999; Hernandez et al. 2000; Dolphin et al. 2002; Weisz et al. 2014).

5.2.2. Leo II

Leo II is also one of the more distant MW companion dwarf spheroidal galaxies (233 kpc, McConnachie 2012). Unlike Leo I, the proper motion study of Leo II reveals that the galactocentric velocity is mostly tangential ($v_{\mathrm{tan}} = 265.2\,\mathrm{km\,s}^{-1}$), with only $21.5\,\mathrm{km\,s}^{-1}$ in the radial direction. Subsequent dynamic modeling of the large velocity and large distance of Leo II suggests that Leo II is most likely passing into the MW halo for the first time (Lépine et al. 2011).

The synthetic MDF of Leo II is best fit by the accretion + truncation model with an accretion parameter of $M = 4.0^{+2.0}_{-2.4}$, a yield of $p = 0.038^{+0.05}_{-0.008}$, and a metallicity cutoff of [Fe/H] $= -1.0$. The simple model underpredicts the number of stars found in the MDF peak and overpredicts the number stars in the metal-poor tail. The accretion model fits the peak and metal-poor tail, but overpredicts the number of stars on the metal-rich end of the distribution, explaining why the best-fit model includes the metallicity truncation term.

Our chemical evolution results are in agreement with Kirby et al. (2011b, 2013), who found the accretion model to be the best fit for Leo II, with an accretion parameter of $M = 3.1^{+0.6}_{-0.5}$ and a yield of $p = 0.028$. For our accretion model we measured $M = 4.1^{+3.0}_{-3.1}$ and $p = 0.038$. Lanfranchi & Matteucci (2010) modeled the detailed chemical evolution of Leo II based on the overall MDF and the α element abundance ratios measured by Shetrone et al. (2009). Their best-fit model predicts one long (7 Gyr) episode of SF starting at 14 Gyr, with a lower SF efficiency than seen in Leo I ($0.3\,\mathrm{Gyr}^{-1}$) and with very high wind efficiency throughout. The chemical evolution of Lanfranchi & Matteucci (2010) is in good agreement with the SFH derived from the wide-field photometric survey of Komiyama et al. (2007). They found that Leo II evolved with a low SF rate up to 8 Gyr ago when SF stopped in the outer regions, and from 8 to 4 Gyr ago the central star-forming region continually shrank until SF essentially stopped.

5.2.3. IC 1613

There have been numerous studies of the gas and stars in IC 1613 (McConnachie 2012), one of the nearest gas-rich dwarf irregular galaxies at a distance of 721 kpc. IC 1613 is similarly distant from M31 (517 kpc); however, it is not considered to be a satellite of either the MW or M31 (McConnachie 2012), and without data on the proper motions the membership of IC 1613 to either is not definitive. Various H I studies have measured the total H I mass as 3–6 $\times 10^7 M_\odot$ (Lake & Skillman 1989; Silich et al. 2006). Additionally, the studies show complicated morphology, including numerous H I arcs, holes, and shells produced from the ongoing SF within IC 1613 as evidenced by the presence of OB associations and H II regions (Garcia et al. 2010).

For IC 1613 we find the accretion + truncation model with an accretion parameter of $M = 3.7^{+2.0}_{-1.9}$, a yield of $p = 0.20^{+0.008}_{-0.036}$, and a cutoff metallicity of [Fe/H] = −0.40 to be the best fit to the synthetic MDF. IC 1613's MDF shows a broad peak at [M/H] = −1.00 and an asymmetric Gaussian shape with an extended metal-poor side of the distribution. The simple model underpredicts the number of stars in the peak, overpredicts the metal-poor tail, and slightly overpredicts the number of stars on the metal-rich side of the MDF. The difference between the accretion model and the accretion + truncation model is small, and almost entirely due to the metal-rich side of the MDF. Since IC 1613 is an isolated galaxy that has a substantial gas mass and shows no sign of interaction, ram pressure stripping cannot be the process truncating the MDF. Instead, the steeper metal-rich side of the MDF reflects the continuing chemical enrichment of IC 1613.

Comparing our work with Kirby et al. (2013) we find that our accretion model with $M = 3.7^{+3.0}_{-1.9}$ and $p = 0.20^{+0.01}_{-0.036}$ has a similar accretion parameter but a higher effective yield compared to their $M = 4.3^{+1.5}_{-1.1}$ and yield of $p = 0.075$. The higher effective yield we measure is potentially due to the different regions of the galaxy sampled. We cover a small (∼5%) central field while the metallicities from Kirby et al. (2013) cover the entire galaxy. Even though our accretion models find similar parameters, Kirby et al. (2013) find that a pre-enriched model has a more likely fit than the accretion model. The pre-enriched model is a generalization of a closed box model that starts with an initial metallicity and does not accrete additional gas over its lifetime.

5.2.4. Phoenix

Phoenix is a transition type galaxy at a distance of 415 kpc and with an absolute V magnitude of −9.9 (McConnachie 2012). There is no H I emission detected within Phoenix itself, however, H I gas has been detected at 4.′5 to 9′ from the center of the galaxy (Young et al. 2007), indicating recent gas expulsion. Young et al. also state that the expelled gas is likely linked with the most recent episode of SF (∼100 Myr ago; Bianchi et al. 2012).

We find the accretion + truncation model to be the best-fit model for the MDF, with an accretion parameter of $M = 3.3^{+2.6}_{-1.6}$, a yield of $p = 0.094^{+0.042}_{-0.018}$, and a cutoff metallicity of [Fe/H] = −0.6. The simple model underpredicts the number of stars in the MDF peak and overpredicts the number of metal-poor stars in the tail of the distribution. The difference between the accretion model and the accretion + truncation is small; both models slightly overpredict the number of metal-poor stars, while on the metal-rich side of the MDF the accretion + truncation model has a slightly better agreement.

Ground-based photometry of Phoenix by Martínez-Delgado et al. (1999) showed the presence of a structurally distinct inner population with mostly young stars in the east–west direction, while isophots of the older component are aligned in the north–south direction. Another ground-based wide-field (26×26 arcmin^2) photometric study shows the young (<1 Gyr) inner population to have a disk-like distribution (Battaglia et al. 2012b). While the accretion + truncation model is found to be the best fit, evidence for ram pressure stripping is not seen in any of the population studies, nor would it be expected in an isolated galaxy.

In a study of the radial SFH properties of dwarf galaxies, Hidalgo et al. (2013) additionally modeled the chemical evolution for Phoenix. Their best-fit model predicts an initial episode of SF lasting 3–4 Gyr with very little or no metal enrichment that accounts for 75% of the total cumulative stellar mass. Additionally, the SF episode is longest in the central regions with shorter SF episodes in the outer regions. To account for the minimal amount of enrichment ([Fe/H] = −1.67) in this first phase, their model predicts a high SFR that would expel most of the metals formed in this episode before they can mix with the ISM. The second phase of SF produces most of the metal enrichment and mainly occurs in the central regions where the gas density is still sufficiently high to support continued SF; they find the metallicity of this burst to be [Fe/H] = −1.08. We find the MDF peak to be [M/H] = −1.17, which is consistent with the enrichment values Hidalgo et al. (2013) found in the central regions of Phoenix from their radial SFH study. However, much like the initial metallicity found by Hidalgo et al. (2013), other photometric studies measured the overall metallicity in Phoenix as ⟨[Fe/H]⟩ ∼ −1.7 (Holtzman et al. 2000), [Fe/H] = −1.9 (Ortolani & Gratton 1988), and ⟨[Fe/H]⟩ = −1.81 ± 0.10 (Held et al. 1999).

6. METALLICITY GRADIENTS

Metallicity gradients found in stellar populations offer clues about past SF as well as interaction history since mergers are thought to remove gradients. Many dwarf galaxies have detectable metallicity gradients (e.g., Fornax, Cetus, Carina, Sculptor, Sextans, Tucana, Leo I, Leo II, Draco, and Andromeda I–III, V, and VI from Harbeck et al. 2001; Tolstoy et al. 2004; Battaglia et al. 2006, 2011, 2012a; Monelli et al. 2012; Kirby et al. 2011a) while others like Ursa Minor and Canes Venatici do not show measurable gradients (Kirby et al. 2011a).

Metallicity gradients can be produced by increased SF (and thus enrichment) in the central regions due to increased gas supply there. The gas density increases with the gravitational potential and thus accumulates toward the centers of galaxies. Additionally, SF is proportional to the gas density, thus producing increased SF and enrichment toward the insides of the galaxy.

Environmental interactions are expected to modify the stellar distributions, diluting any gradients and possibly inducing morphological transformations (Łokas et al. 2012). Additionally, recent simulations of the chemo-dynamical evolution of dwarf galaxies have shown tidal interactions to be an efficient mechanism to remove metallicity gradients (Nichols et al. 2014). Also, observations by Hidalgo et al. (2013) have

Table 5
Metallicity Gradients

Galaxy Name	d[M/H]/$d\theta$ (dex deg^{-1})	d[M/H]/dr (dex kpc^{-1})	d[M/H]/$d(r/r_h)$ (dex per r_h)
Leo I	−1.52	−0.34	−0.086 ± 0.04
Leo II	−11.55	−3.02	−0.54 ± 0.10
IC 1613	−2.48	−0.20	−0.29 ± 0.29
Phoenix	−1.84	−0.26	−0.11 ± 0.20

shown that radial SFHs and metallicity gradients are consistent with the SF in dwarf galaxies being quenched in the outer regions due to limited gas availability.

Gradients in age and metallicity have been seen for a wide range of physical characteristics of dwarf galaxies. The trend of younger and higher metallicity stars increasing toward the centers of galaxies spans many galactic properties such as total mass, gas mass, metallicity, velocity dispersion, and environment. The fact that gradients are consistently found even across a wide range of physical characteristics hints that population gradients are intrinsic to dwarf galaxy formation and evolution. However, at large radii, many of these differences tend to disappear, suggesting some physical processes may not equally affect all galactocentric radii (e.g., the UV background could affect the inner and outer regions differently).

The radial metallicity gradients we measured are reported in Table 5 and shown in Figure 8. We find metallicity gradients in Leo I and Leo II. In Phoenix and IC 1613 the errors on the gradients are consistent with no slope. Much of the error is due to the small radial extent that the WFC3 field of view covers in these galaxies, and thus we cannot confirm or rule out a metallicity gradient in Phoenix or IC 1613.

In Leo I the age and metallicity gradients have been seen in various SF histories, variable star populations, and metallicity studies. Held et al. (2010) found evidence for a radial gradient in the 1–3 Gyr stellar population using near-IR photometry. Gullieuszik et al. (2009) found a shallow metallicity gradient of −0.27 dex kpc^{-1} as part of their metallicity study of Leo I, which is shallower than the gradient we measure, −0.34 dex kpc^{-1}, in the same units. In the work by Kirby et al. (2011b), gradients for Leo I are reported as d[Fe/H]/$d(r/r_c)$ = −0.11 dex per r_c, while we find a similar gradient for Leo I of −0.09 ± 0.07 dex per r_h, where the core radius (r_c = 240 pc) or the half-light radius (r_h = 251 pc) both give the same gradient value to two significant figures. Our photometry covers Leo I out to ∼0.7 r_h, while the work by Kirby et al. (2011b) extends ∼4 times farther for Leo I.

In Leo II, the wide-field photometric survey by Komiyama et al. (2007) found evidence of a radial gradient in the HB morphology, where red HB stars are more centrally concentrated than blue HB stars. In the work by Kirby et al. (2011b) the gradient for Leo II is reported as d[Fe/H]/$d(r/r_c)$ −0.21 dex per r_c, while we find a steeper gradient of −0.54 ± 0.10 dex per r_h, where the core radius (r_c=180 pc) and the half-light radius (r_h = 176 pc) both give the same gradient value to two significant figures. Our photometry covers Leo II out to about 0.6 r_h, while the work by Kirby et al. (2011b) extends ∼3 times farther.

In IC 1613 the wide-field photometric study of Bernard et al. (2007) looked at radial differences in the CMDs and concluded that there is an age gradient; however, they could not confirm a metallicity gradient in IC 1613 from their broadband ground-based photometry.

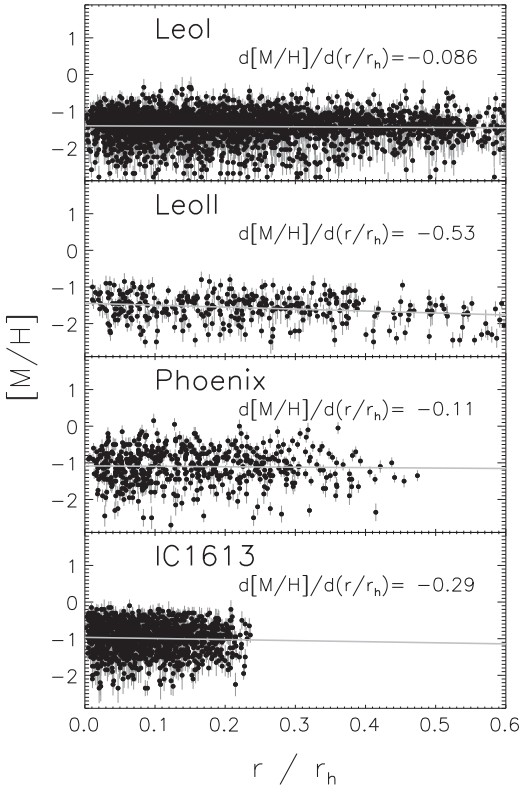

Figure 8. Gradients are in units of dex of [M/H] per r_h, where r_h is the half-light radius as defined by McConnachie (2012).

The radial SFH study of Phoenix by Hidalgo et al. (2009, 2013) measured the radial SF in Phoenix while simultaneously deriving metallicities. They found that Phoenix had longer periods of SF in the central regions and decreasing average metallicities as a function of radius, with the central regions having an average [Fe/H] ∼ −1.4, decreasing outward to −1.7, although they do not quantify a metallicity gradient for the galaxy.

7. DISCUSSION

7.1. Morphological Transitions and Implications from the MDFs and CEM

As the name suggests, a dwarf transition galaxy is considered to be in a state of morphological transition between a dIr and dSph type galaxy (Lin & Faber 1983; Mayer et al. 2001; Grebel et al. 2003; Kazantzidis et al. 2011). This idea is supported by the presence of the morphology–density relationship, where dSphs are mainly found in dense environments close to a much larger primary while dIrs and dTrans are found in isolation (Weisz et al. 2011b). The dwarf galaxy morphology segregation has led to an environment-dependent explanation invoking tidal stirring and ram pressure stripping to transform a dIr close to a larger galaxy into a dTrans then a dSph over subsequent orbital passages around the primary (Mayer et al. 2007; Peñarrubia et al. 2008; Kazantzidis et al. 2011).

However, some dwarf galaxy properties conflict with the morphological transition scenario. DTrans have gas fractions (Weisz et al. 2011a) and UV fluxes (Lee et al. 2011) similar to

dIrs, while the Hα emission in dTrans is markedly less and the typical stellar mass of dTrans is ~3–4 times lower than that of dIrs. DTrans are mostly located in isolated regions (like dIrs), but dTrans luminosities, like dSphs, are lower than dIrs. This led Weisz et al. (2011a) to suggest that dTrans appear to be lower mass versions of dIrs that lack recent SF, and not an evolutionary bridge between dSphs and dIrs. Additionally, should dTrans be progenitors of dSphs then they should be seen in locations similar to both dSph and dIrs, but they are found only in the same regions as dIrs.

Further evidence against a morphological transition theory comes from Kirby et al. (2013), who found systematic differences in the MDF shapes of dIrs and dSphs. They found that the dSph MDF shapes were systematically narrower and more peaked while dIrs tend to have wider MDFs that more closely resemble a simple chemical evolution model. The narrower dSph MDF is best fit by CEMs with large amounts of accretion, which is at odds with the proposed mechanism to transform dIrs into dSphs, i.e., gas stripping.

Accretion has been shown to be an important component in dwarf galaxy evolution (Brook et al. 2014). Also, the analytical "Best Accretion" model of Lynden-Bell (1975) implies that dSphs tend to require large accretion parameters (M values) to fit the observed MDFs (Kirby et al. 2013). However, the morphology–density relation points to gas stripping and tidal disruption as important factors in shaping dSphs. Simulations have also shown that gas stripping and tidal disruption are integral in creating many of the the dSphs seen today (Mayer et al. 2006). Further examination of the Best Accretion model of Lynden-Bell (1975) shows that there is no physical basis behind the form of Equation (3) other than that it produces the desired MDF shapes. Equation (3) simply assumes a nonlinear relation between gas mass and the stellar mass that follows a quadratic relation that peaks then decays as a function of stellar mass. Due to the contradictory implications from the accretion model and the gas stripping caused by gravitational interactions known to be integral in shaping dSphs, in addition to the lack of physical meaning behind the functional form of the accretion model we suggest that the interpretation of the accretion portion of the accretion model should be left for more sophisticated CEMs. In lieu of drawing interpretations from the models themselves, we can use the differences in the model parameters in the context of the dynamic histories of each galaxy to inform our discussion.

Examining the dSph type galaxies in our sample (Leo I and II), we find that the MDF of Leo II is more similar to the MDFs from IC 1613 (dIr) and Phoenix (dTrans) than to Leo I's. Leo II is also one of the more distant dSphs associated with the MW (233 kpc), although it is slightly closer than Leo I (254 kpc; McConnachie 2012). Dynamical studies of Leo II (Koch et al. 2007b) and wide-field photometric studies (Coleman et al. 2007) show no significant signs of tidal distortion. Lépine et al. (2011) studied Leo II's proper motion and found nearly all of its velocity is in a tangential component ($v_{\rm tan} = 265.2$ km s^{-1}) with only a small radial component ($v_{\rm rad} = 21.5$ km s^{-1}). Lépine et al. (2011) take this to mean that Leo II either has a low-eccentricity orbit, or is near perigalacticon or apogalacticon, and the lack of evidence for tidal disruptions (Coleman et al. 2007; Koch et al. 2007b) likely rules out the latter.

Currently the only known mechanism to transform a rotating dIr into a dSph is through gravitational influence from a larger primary (Mayer et al. 2001). Consequently, it can be assumed that Leo II has experienced some tidal interactions with the MW in the past. However, Leo II shows no signs of dynamical interactions, beside the fact that it is a dSph. Moreover, the similarity of the MDFs of Leo II, IC 1613, and Phoenix suggests that these galaxies experienced comparable conditions during their chemical evolution. Since IC 1613 and Phoenix are isolated and evolved without outside influence, it could be inferred that Leo II also chemically evolved without dynamical influence from the MW. The SFH of Leo II shows that 95% of the stars were formed over 6.3 Gyr ago (Weisz et al. 2014); with so many of the stars formed at early times, Leo II has had ample time to be transformed from a disk to a spheroid after most of the chemical evolution occurred. We do find the accretion + truncation model to be the best fit for Leo II, where the cutoff on the metal-rich side of Leo II's MDF is shallower than predicted from the accretion model. We interpret this as an indication of ram pressure stripping; however, in Leo II, the cutoff is not nearly as drastic as in Leo I, indicating that most of the chemical evolution had occurred before the MW began stripping and truncating Leo II's SF. While this is by no means direct proof, the evidence supports the idea that Leo II chemically evolved without strong dynamical influence from the MW.

Leo I on the other hand shows evidence of strong tidal interactions with the MW. The proper motions and dynamic modeling of Leo I show that it passed into the MW's potential 2.33 Gyr ago, reaching its pericentric approach 1.05 Gyr ago (Mateo et al. 2008; Sohn et al. 2013). Additionally, the dynamic results correlate well with the CMD-based SFHs. Leo I shows slow ancient SF with an increase to its highest rate 2–3 Gyr ago, after which the galaxy stopped forming stars 1 Gyr ago (Caputo et al. 1999; Gallart et al. 1999; Hernandez et al. 2000; Dolphin et al. 2002; Weisz et al. 2014). Sohn et al. (2013) suggest that the increased SF at 3 Gyr and the abrupt stop at 1 Gyr could have been caused by ram pressure compression or gravitational torques exerted by the MW as the galaxy passed into the MW's potential. For Leo I, the dynamical history has had a significant impact on the SFH, and by extension on the chemical evolution.

We interpret the sharp difference in the M parameters along with the dynamic information in the literature on Leo I, Leo II, IC 1613, and Phoenix, as possible evidence that the galaxies chemically evolved under different conditions. The first is passive chemical evolution, where gas-rich, star-forming galaxies (i.e., dIrs) gradually truncate their SF as the gas supply is exhausted, evolving into a dTrans and producing a broad MDF in the process. This type of evolution is what is most likely seen in Leo II (dSph), Phoenix (dTrans), and IC 1613 (dIr) at various stages in the process. Leo II formed the majority of its stars over 6 Gyr ago and the MDF suggests it chemically evolved without significant interactions before it was transformed into a dSph by the MW. Phoenix appears to be in the process of passively evolving; the dynamics and SFH show no indication of interaction. Instead, the SFH shows a slow decrease in SF up to a few 100 Myr ago when SF stopped. Additionally, IC 1613 is isolated from both the MW and M31 and does not show dynamical evidence of interactions, and the MDF of IC 1613 is similar in shape to Leo II and Phoenix. It is known that dSphs are created through the gravitational influence of a larger primary; if the interaction occurs concurrently with the chemical evolution it will be reflected

in the MDF. Previous studies have shown that the MW's influence on Leo I is reflected in the SFH and dynamics; we are suggesting it is also shown in the narrow MDF.

7.2. MDF Evolution

One understated assumption in analytic CEMs is that each model represents the end point of that galaxy's evolution. However, dIrs and dTrans are not at the end of their chemical evolution since they are still forming stars and enriching the ISM. Therefore, we must take care when comparing the MDFs of active galaxies such as IC 1613 and Phoenix to the dSphs like Leo I and II, which, arguably, have completed their chemical evolution 1 to 6 Gyr ago, respectively. Additionally, for dSphs the morphology–density relation suggests that the removal of gas interrupted the chemical evolution, altering the chemistry to no longer reflect the end state of CEMs.

These various endpoints can be seen in our galaxy sample. Leo I shows an MDF truncated on the metal-rich side, indicative of halted chemical evolution. Leo II shows signs of mild truncation, as the CEM slightly overpredicts the number of metal-rich stars and the accretion + truncation model was the best-fit model for Leo II. As we discussed previously, Leo II is within the virial radius of the MW, but has a mostly circular orbit at a large distance; therefore it has been weakly affected by the MW's gravity, as the mild truncation shows.

As a dIr, IC 1613 is still actively forming stars and enriching its ISM; therefore we would not expect the MDF to reflect a fully completed chemical evolution. The ongoing enrichment in IC 1613 manifests itself with fewer metal-rich stars than predicted by the CEM.

Phoenix, on the other hand, is the only galaxy to nearly match the metal-rich end of the CEM. Phoenix is a transition galaxy that expelled its last remaining gas reserves with a final burst of SF ∼100 Myr ago (Young et al. 2007). The isolated location and apparent exhaustion of gas imply that Phoenix has completed its chemical evolution.

One other consideration is that our field of view is small for all of the galaxies in our sample (covering 5%–20% of the various galaxies). Given that many dwarf galaxies show metallicity gradients and variations in SFH as a function of radius, the MDFs will also change as a function of radius, and the solutions to the CEMs cannot be applied to the entire galaxy.

8. CONCLUSION

We measured the MDFs of Leo I, Leo II, IC 1613, and Phoenix dwarf galaxies by measuring individual stellar metallicities and by modeling the stellar population to create synthetic MDFs for each galaxy. We find the synthetic MDFs to be a better representation of the overall metallicity distribution, because this method reduces the photometric scatter propagated into the photometric metallicities.

We fit each MDF with a CEM. We find the simple model to be a poor fit for all of our dwarf galaxies, while the accretion + truncation model is the best fit for the synthetic MDFs for all four of the galaxies. The fact that all of our galaxies are best fit by the accretion + truncation model reflects the fact that most galaxies do not make it to the natural completion of the chemical evolution, either because they are still actively forming stars (dIrs) or because they were truncated by other processes such as ram pressure stripping (dSphs).

We find a similar accretion parameter, ($M \sim 4$), for Leo II, IC 1613, and Phoenix despite the fact that they all have different masses, SFH, morphologies, and average metallicities. We interpret the resemblance of their MDFs as an indication that their chemical evolutions occurred under similar conditions, which indicates that Leo II completed most of its chemical evolution in isolation before it was significantly tidally disrupted and transformed into a dSph type galaxy by the MW.

Leo I has the narrowest MDF, a much larger accretion parameter, and shows significant evidence for interactions with the MW at the same time as the galaxy was forming stars and chemically evolving. We suggest that the MDFs can reveal dynamical interactions if they occur in concert with SF and chemical evolution, or if the galaxy chemically evolved in relative isolation. The narrower MDFs are indicative of interactions shaping the galaxy's current morphology, while a broader MDF indicates a passive evolution. The differences in the MDFs could be a way to distinguish between the two formation pathways. To further this theory we would need to examine the MDFs and dynamic histories of many LG dwarf galaxies.

Additionally, we measured metallicity gradients for Leo I and Leo II. We see some evidence of gradients in Phoenix and IC 1613; however, our data do not cover the radial extent required to determine a metallicity gradient greater than the error bars.

Support for program 12304 was provided by NASA through a grant from the Space Telescope Science Institute, which is operated by the Association of Universities for Research in Astronomy, Inc., under NASA contract NAS 5-26555.

REFERENCES

Battaglia, G., Irwin, M., Tolstoy, E., de Boer, T., & Mateo, M. 2012a, ApJL, 761, L31
Battaglia, G., Rejkuba, M., Tolstoy, E., Irwin, M. J., & Beccari, G. 2012b, MNRAS, 424, 1113
Battaglia, G., Tolstoy, E., Helmi, A., et al. 2006, A&A, 459, 423
Battaglia, G., Tolstoy, E., Helmi, A., et al. 2011, MNRAS, 411, 1013
Bernard, E. J., Aparicio, A., Gallart, C., Padilla-Torres, C. P., & Panniello, M. 2007, AJ, 134, 1124
Bianchi, L., Efremova, B., Hodge, P., Massey, P., & Olsen, K. A. G. 2012, AJ, 143, 74
Bosler, T. L., Smecker-Hane, T. A., & Stetson, P. B. 2007, MNRAS, 378, 318
Brook, C. B., Stinson, G., Gibson, B. K., et al. 2014, MNRAS, 443, 3809
Caputo, F., Cassisi, S., Castellani, M., Marconi, G., & Santolamazza, P. 1999, AJ, 117, 2199
Coleman, M. G., Jordi, K., Rix, H.-W., Grebel, E. K., & Koch, A. 2007, AJ, 134, 1938
Dolphin, A. E. 2000, PASP, 112, 1383
Dolphin, A. E. 2002, in ASP Conf. Ser. 274, Observed HR Diagrams and Stellar Evolution, ed. T. Lejeune, & J. Fernandes (San Francisco, CA: ASP), 450
Dotter, A., Chaboyer, B., Jevremović, D., et al. 2008, ApJS, 178, 89
Gallart, C., Freedman, W. L., Aparicio, A., Bertelli, G., & Chiosi, C. 1999, AJ, 118, 2245
Garcia, M., Herrero, A., Castro, N., Corral, L., & Rosenberg, A. 2010, A&A, 523, A23
Grcevich, J., & Putman, M. E. 2009, ApJ, 696, 385
Grebel, E. K., Gallagher, J. S., III, & Harbeck, D. 2003, AJ, 125, 1926
Gullieuszik, M., Held, E. V., Rizzi, L., et al. 2008, MNRAS, 388, 1185
Gullieuszik, M., Held, E. V., Saviane, I., & Rizzi, L. 2009, A&A, 500, 735
Harbeck, D., Grebel, E. K., Holtzman, J., et al. 2001, AJ, 122, 3092
Harrington, R. G., & Wilson, A. G. 1950, PASP, 62, 118
Held, E. V., Gullieuszik, M., Rizzi, L., et al. 2010, MNRAS, 404, 1475
Held, E. V., Saviane, I., & Momany, Y. 1999, A&A, 345, 747
Hendricks, B., Koch, A., Lanfranchi, G. A., et al. 2014, ApJ, 785, 102

Hernandez, X., Gilmore, G., & Valls-Gabaud, D. 2000, MNRAS, 317, 831
Hidalgo, S. L., Aparicio, A., Martínez-Delgado, D., & Gallart, C. 2009, ApJ, 705, 704
Hidalgo, S. L., Monelli, M., Aparicio, A., et al. 2013, ApJ, 778, 103
Holtzman, J. A., Smith, G. H., & Grillmair, C. 2000, AJ, 120, 3060
Kazantzidis, S., Łokas, E. L., Callegari, S., Mayer, L., & Moustakas, L. A. 2011, ApJ, 726, 98
Kirby, E. N., Cohen, J. G., Guhathakurta, P., et al. 2013, ApJ, 779, 102
Kirby, E. N., Cohen, J. G., Smith, G. H., et al. 2011a, ApJ, 727, 79
Kirby, E. N., Lanfranchi, G. A., Simon, J. D., Cohen, J. G., & Guhathakurta, P. 2011b, ApJ, 727, 78
Koch, A., Feltzing, S., Adén, D., & Matteucci, F. 2013, A&A, 554, A5
Koch, A., Grebel, E. K., Kleyna, J. T., et al. 2007a, AJ, 133, 270
Koch, A., Kleyna, J. T., Wilkinson, M. I., et al. 2007b, AJ, 134, 566
Komiyama, Y., Doi, M., Furusawa, H., et al. 2007, AJ, 134, 835
Kroupa, P. 2001, MNRAS, 322, 231
Lake, G., & Skillman, E. D. 1989, AJ, 98, 1274
Lanfranchi, G. A., & Matteucci, F. 2010, A&A, 512, A85
Lee, H., Skillman, E. D., Cannon, J. M., et al. 2006, ApJ, 647, 970
Lee, J. C., Gil de Paz, A., Kennicutt, R. C., Jr., et al. 2011, ApJS, 192, 6
Lemasle, B., de Boer, T. J. L., Hill, V., et al. 2014, A&A, 572, A88
Lépine, S., Koch, A., Rich, R. M., & Kuijken, K. 2011, ApJ, 741, 100
Lin, D. N. C., & Faber, S. M. 1983, ApJL, 266, L21
Łokas, E. L., Majewski, S. R., Kazantzidis, S., et al. 2012, ApJ, 751, 61
Lynden-Bell, D. 1975, VA, 19, 299
Marcolini, A., D'Ercole, A., Battaglia, G., & Gibson, B. K. 2008, MNRAS, 386, 2173
Marcolini, A., D'Ercole, A., Brighenti, F., & Recchi, S. 2006, MNRAS, 371, 643
Martínez-Delgado, D., Gallart, C., & Aparicio, A. 1999, AJ, 118, 862
Mateo, M., Olszewski, E. W., & Walker, M. G. 2008, ApJ, 675, 201
Mateo, M. L. 1998, ARA&A, 36, 435
Mayer, L., Governato, F., Colpi, M., et al. 2001, ApJ, 559, 754
Mayer, L., Kazantzidis, S., Mastropietro, C., & Wadsley, J. 2007, Natur, 445, 738
Mayer, L., Mastropietro, C., Wadsley, J., Stadel, J., & Moore, B. 2006, MNRAS, 369, 1021
McConnachie, A. W. 2012, AJ, 144, 4
Monelli, M., Bernard, E. J., Gallart, C., et al. 2012, MNRAS, 422, 89
Nichols, M., Revaz, Y., & Jablonka, P. 2014, A&A, 564, A112
Ordoñez, A. J., Yang, S.-C., & Sarajedini, A. 2014, ApJ, 786, 147
Ortolani, S., & Gratton, R. G. 1988, PASP, 100, 1405
Pagel, B. E. J. 1997, Nucleosynthesis and Chemical Evolution of Galaxies
Peñarrubia, J., Navarro, J. F., & McConnachie, A. W. 2008, ApJ, 673, 226
Prantzos, N. 2008, A&A, 489, 525
Revaz, Y., Jablonka, P., Sawala, T., et al. 2009, A&A, 501, 189
Ross, T. L., Holtzman, J. A., Anthony-Twarog, B. J., et al. 2014, AJ, 147, 4
Shetrone, M., Venn, K. A., Tolstoy, E., et al. 2003, AJ, 125, 684
Shetrone, M. D., Côté, P., & Sargent, W. L. W. 2001, ApJ, 548, 592
Shetrone, M. D., Siegel, M. H., Cook, D. O., & Bosler, T. 2009, AJ, 137, 62
Silich, S., Lozinskaya, T., Moiseev, A., et al. 2006, A&A, 448, 123
Skillman, E. D., Tolstoy, E., Cole, A. A., et al. 2003, ApJ, 596, 253
Skillman, E. D., Hidalgo, S. L., Weisz, D. R., et al. 2014, ApJ, 786, 44
Sohn, S. T., Besla, G., van der Marel, R. P., et al. 2013, ApJ, 768, 139
Spekkens, K., Urbancic, N., Mason, B. S., Willman, B., & Aguirre, J. E. 2014, ApJL, 795, L5
Starkenburg, E., Hill, V., Tolstoy, E., et al. 2013, A&A, 549, A88
Tautvaišienė, G., Geisler, D., Wallerstein, G., et al. 2007, AJ, 134, 2318
Tolstoy, E., Hill, V., & Tosi, M. 2009, ARA&A, 47, 371
Tolstoy, E., Irwin, M. J., Helmi, A., et al. 2004, ApJL, 617, L119
Tolstoy, E., Venn, K. A., Shetrone, M., et al. 2003, AJ, 125, 707
Weisz, D. R., Dolphin, A. E., Dalcanton, J. J., et al. 2011a, ApJ, 743, 8
Weisz, D. R., Dolphin, A. E., Skillman, E. D., et al. 2014, ApJ, 789, 147
Weisz, D. R., Dalcanton, J. J., Williams, B. F., et al. 2011b, ApJ, 739, 5
Young, L. M., Skillman, E. D., Weisz, D. R., & Dolphin, A. E. 2007, ApJ, 659, 331